Journal of ELECTRONIC MATERIALS, Vol. 48, No. 7, 2019
https://doi.org/10.1007/s11664-019-07174-x
© 2019 The Minerals, Metals & Materials Society

Preparation of Eu-Doped Cu_2O Thin Films Using Different Concentrations by SILAR and Their Heterojunction Property with ZnO

N. SOUNDARAM,[1] R. CHANDRAMOHAN,[1] R. DAVID PRABU,[2] S. VALANARASU,[3,7] K. JEYADHEEPAN,[4] A. KATHALINGAM,[5] MOHAMED S. HAMDY,[6] ABDULLAH M. ALHANASH,[6] and K.S. AL-NAMSHAH[6]

1.—Department of Physics, Sree Sevugan Annamalai College, Devakottai 630303, India. 2.—Department of Physics, Loyola College of Arts and Science, Oilpatti, Mettala, Namakkal (Dt), India. 3.—PG and Research Department of Physics, Arul Anandar College, Karumathur, Madurai 625514, India. 4.—Multifunctional Materials and Devices Lab, Anusandhan Kendra – II, School of EEE, SASTRA University, Tirumalaisamudram, Thanjavur 613 401, India. 5.—Millimeter-Wave Innovation Technology Research Center (MINT), Dongguk University-Seoul, Seoul 04620, Republic of Korea. 6.—Chemistry Department, College of Science, King Khalid University, P.O. Box 9004, Abha 61413, Saudi Arabia. 7.—e-mail: valanroyal@gmail.com

Europium-doped Cu_2O thin films were prepared by simple successive ionic layer adsorption and reaction (SILAR) with different Eu doping concentrations: 1%, 3% and 5%. The effect of doping level on structural, optical, surface morphological and electrical properties of the films were studied by x-ray diffraction analysis, UV–Vis spectroscopy, scanning electron microscopy and Hall effect measurements, respectively. Crystallite size, dislocation density, microstrain and texture coefficient of the films were estimated using x-ray diffraction data. The crystallite size was found to vary between 27 nm and 21 nm for the change of doping percentage 1–5%. Morphology of Eu:Cu_2O and ZnO films had cauliflower and hexagonal shapes, respectively, without any cracks. Optical studies done on the films revealed an increase of band gap as 2.08 eV, 2.26 eV and 2.41 eV for Eu doping concentrations of 1%, 3% and 5%, respectively. The ZnO film showed a maximum of 80% transmittance and band gap of 3.20 eV. Photoluminescence (PL) studies revealed two emission peaks centered at 394 nm and 377 nm for the Eu:Cu_2O and ZnO films, respectively. Eu:Cu_2O/ZnO heterojunction solar cells were also prepared and their properties studied; they were found to show increased open circuit voltage and short circuit current for 5% Eu doping concentration.

Key words: Eu-doped Cu_2O, ZnO, heterostructure, solar cell efficiency, SILAR

INTRODUCTION

Cuprous oxide (Cu_2O) is a promising material for photovoltaic applications. Its interest lies on the abundant availability, non-toxicity and easy process ability of the material.[1] Other interesting features of Cu_2O are large minority carrier diffusion length (2–12 μm), large binding energy of excitons, direct band gap energy of 2.1–2.6 eV with high absorption in the visible spectrum, which are more suitable for solar energy conversion.[2] Although Cu_2O has 20% conversion efficiency according to Shockley–Queisser criteria (SQC), the currently reported efficiency of Cu_2O-based heterojunction devices remains low.[3,4] This poor response is caused by intrinsic

(Received November 14, 2017; accepted March 28, 2019; published online April 11, 2019)

defects, increased carrier recombination and decreased minority carrier diffusion.[5,6] Cu_2O is intrinsically a *p*-type semiconductor, and it is challenging to create a *p*–*n* homojunction using Cu_2O, whereas ZnO is considered the best option to fabricate heterojunction solar cells with Cu_2O.[7] To increase the values of V_{oc} and J_{sc} of Cu_2O/ZnO solar cells, different modalities are followed. Use of high surface area nanotubes or nanorods can reduce the conduction and recombination losses.[8] Passivation of the surface reduces surfacial defects increasing photoresponse of solar cells.[9] Doping is a promising technique used to increase the carrier concentration and electronic and optical properties, and thus photoconversion efficiency is improved.[10] Different dopants such as KCl,[11] N,[12] F, Cl, and Br[13] are used. Rare earth elements are attractive as potential dopants to improve the solar cell efficiencies.[14] Amongst various rare earth dopants, europium (Eu) is considered an efficient dopant.[15,16] The Eu^{2+} ion can act as a down-conversion center by absorbing sunlight at 334 nm and re-emitting at above 400 nm, a suitable region for solar cell response.[17,18] Hence, Eu doping can increase the power conversion efficiency of solar cells.[19] To the best of our knowledge, no report is available on Eu-doped Cu_2O thin films synthesized by successive ionic layer adsorption and reaction (SILAR). In this paper, we investigate the structural, optical and electrical properties of Eu:Cu_2O thin films, and its solar cell property by forming a heterojunction with ZnO.

EXPERIMENTAL PROCEDURE

Eu-doped Cu_2O thin films were prepared by SILAR on glass substrates. Highly pure copper sulphate pentahydrate ($CuSO_4·5H_2O$), sodium thiosulphate ($Na_2S_2O_3·5H_2O$) and sodium hydroxide (NaOH) were used as a host copper precursor, complexing and oxidizing agents, respectively. Samples of 1 M of copper sulphate and sodium thiosulphate were dissolved in double-distilled water (100 mL) in a 1:5 volumetric ratio and stirred for 10 min at room temperature to get well-dissolved and clear transparent solution with pH $\sim$ 11. Another solution of 1 M NaOH was prepared in a beaker and maintained at 70°C. In total, three beakers of different solutions were used to deposit as follows. Firstly, a well cleaned glass substrate was vertically dipped into the hot NaOH solution for 20 s. In the second step the substrate was dipped in 1 M $CuSO_4·5H_2O$ for 20 s to enable copper ions in the solution to adsorb at the substrate surface. The copper-coated substrate was finally dipped into the double-distilled water for 10 s to remove the loosely adsorbed copper ions. This process was repeated several times ($\sim$ 100) to get the expected thickness. After the deposition process, the coated films were dried for 1 h in air at room temperature. Furthermore, the same procedure was applied to prepare europium-doped copper oxide thin films with different doping concentrations (1 at.%, 3 at.% and 5 at.%). The dopant precursor solution [$Eu(NO_3)_3·5H_2O$] was added to a 1 M copper sulphate solution. SILAR deposition of ZnO thin films was done using 0.1 M zinc sulphate as the zinc source and 0.1 M NaOH as the complexing agent. ZnO seed layer was prepared by a three-step process viz: (1) immersing the substrates into sodium zincate bath; (2) reaction in hot water at 90°C to form ZnO layer; (3) drying the substrates in air. The cycles depicted above were performed for a known number of times to obtain the desired film thickness. Al metal paste in dots of 2-mm diameter were used for electrical contacts to measure current–voltage response of the devices.

Film Characterization

Thickness of the prepared films was measured using a Stylus Profilometer. X-ray diffraction was used to study the structural properties of the prepared films using CuKα radiation. Scanning electron microscopy (Model JSM-6320F, JEOL, Tokyo, Japan) was used to analyze the morphology of the films. Optical absorption measurements were performed using a Shimadzu UV-3101PC spectrophotometer in the UV–Visible range (200–2400 nm). Room temperature photoluminescence spectra of Eu:Cu_2O and ZnO films were observed using a Perkin Elmer LS55 florescent spectrophotometer with an excitation source of wavelength 325 nm. Hall Effect measurement was done at room temperature to observe the electrical resistivity of the prepared films. *I*–*V* characterization of the fabricated *n*-ZnO/*p*-Cu_2O heterojunction was done under dark and 300 W halogen lamp-illuminated conditions.

RESULTS AND DISCUSSIONS

XRD Analysis

XRD pattern of Eu doped Cu_2O films prepared using SILAR technique are shown in Fig. 1a. It reveals polycrystalline nature of the films with a preferred (111) orientation together with (1 1 0), (2 0 0), (2 2 0), (3 1 1) and (2 2 2) peaks. The position of the diffraction peaks fit well with the cubic structure (JCPDS Card No. 65-3288).[20,21] There are no other new peaks corresponding to europium oxide or related secondary and impurity phases. Peaks are slightly shifted as the Eu doping percentage is increased as shown in Fig. 1b. The observed peak intensity is significantly decreased along with the increasing of doping concentration causing loss of crystallinity due to lattice distortion.[22] The inclusion of Eu^{3+} ions into the Cu_2O lattice induces strain ensuing change of lattice periodicity and decrease in crystal symmetry without affecting its volume. XRD peak profiling for the high intensity peak (111) was carried out for the investigated samples to

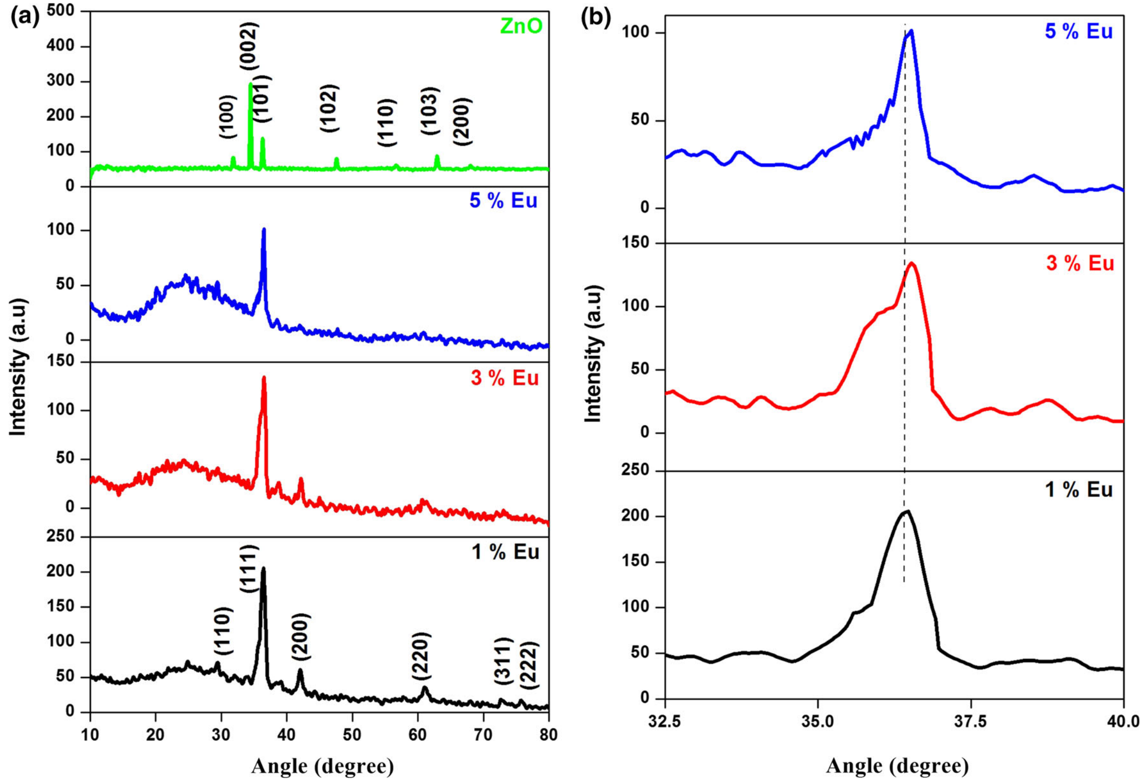

Fig. 1. (a) XRD patterns of Eu doped Cu_2O and ZnO samples prepared by SILAR. (b) Peak shift for Eu doped Cu_2O thin films in the XRD spectra.

determine broadening parameter (β), a main parameter to calculate the size of the crystallite. The size of crystallite D was determined from the relation (1).[23]

$$D = \frac{0.9\lambda}{\beta \cos\theta} \tag{1}$$

where λ is wavelength of x-rays, D is crystallite size, β is full-width at half-maximum (FWHM) value of x-ray diffraction peaks. The diffraction peaks are broadened as the Eu^{+3} concentration is increased; this suggests that there is a systematic decrease in crystallite size. As expected, the strain in crystal is increased as the doping concentration is increased. Microstrain and dislocation density of the films were determined using the following equations.[24]

$$\varepsilon = \frac{\beta \cos\ \theta}{4} \tag{2}$$

$$\delta = \frac{1}{D^2} \tag{3}$$

The microstrain and dislocation densities are increased with doping concentration. This increase of microstrain and dislocation density indicates the increase of doping induced defects generated in Cu_2O lattice. The lower strain (ε) and small dislocation density (δ) values obtained for 1% Eu-doped Cu_2O films indicate the good crystallization level with decreased defect levels.

The stacking fault probability with peak shift $\Delta(2\theta)$ is given by the relation (4)

$$\alpha = \left[\frac{2\pi^2}{45\sqrt{3}}\right]\left[\frac{\Delta(2\theta)}{\tan\theta_{311}}\right] \tag{4}$$

The stacking fault is a type of defect which characterizes the disorder of the prepared Cu_2O thin films. It mainly depends on the position of peaks and it is found as minimum for undoped Cu_2O films (see Table I).

The texture coefficient (TC) value of the films was calculated for the preferred orientation using the following relation.[25]

$$\mathrm{TC}(hkl) = \frac{I(hkl)/I_0(hkl)}{N_r^{-1}\sum I(hkl)/I_0(hkl)} \tag{5}$$

where $I_{(hkl)}$ is the measured intensity, $I_{0(hkl)}$ is the ASTM standard intensity value and N is the number of diffraction planes. The observed TC values of Eu-doped Cu_2O thin films are given in the Table I. The texture coefficient of predominant (111) plane is also found to decrease with the increase of Eu concentration. X-ray diffraction pattern of SILAR deposited ZnO film is also shown in Fig. 1. The observed XRD pattern corresponds to the JCPDS card no [36-1451] indicating the formation of polycrystalline hexagonal phase of ZnO.

Table I. Thickness and structural parameters of Eu doped Cu_2O and ZnO thin films

Sample	Europium (%)	Thickness (μm)	Crystallite size (nm)	Microstrain (ε) × 10^3	Dislocation density (δ) × 10^{15}	Stacking fault probability ($\alpha \times 10^{-3}$)	Texture coefficient TC (*hkl*)
Cu_2O	1	0.97	27	0.45	1.372	1.20	1.72
	3	0.88	24	0.58	1.736	1.37	1.38
	5	0.75	21	0.67	2.267	1.58	1.12
ZnO	–	0.82	31	0.40	1.041	1.05	1.76

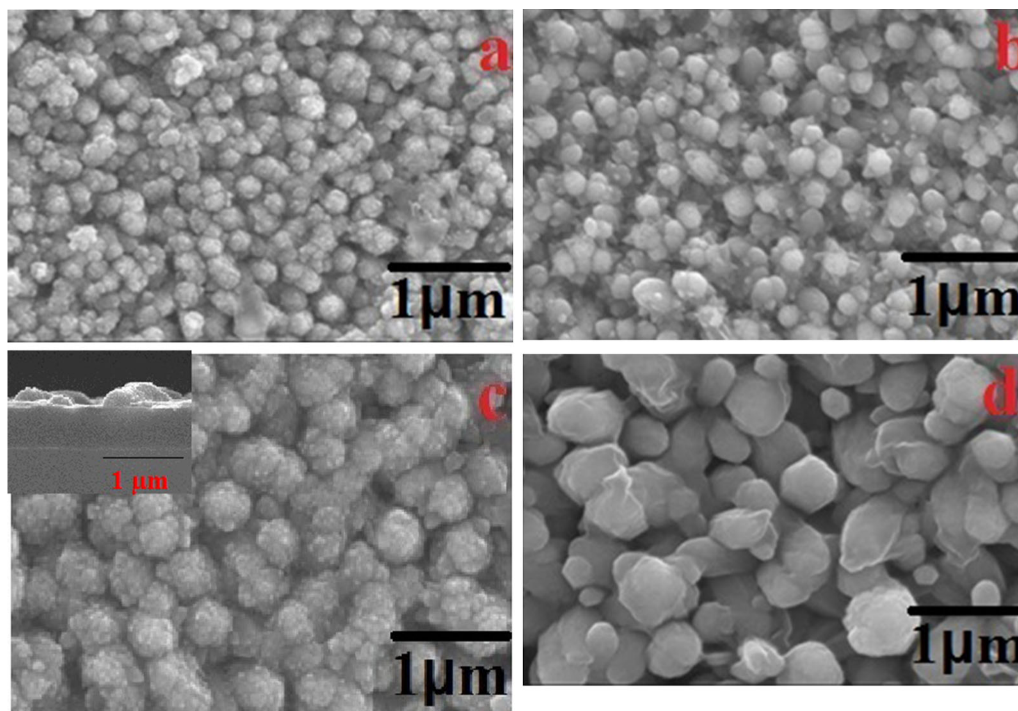

Fig. 2. SEM micrographs of Eu: Cu_2O samples. (a) 1% Eu, (b) 3% Eu, (c) 5% Eu and (d) ZnO thin films.

This study indicates that the overall structure of the Cu_2O films is not altered due to Eu doping. However minor changes do occur inside the lattice arrangements. The microstrain variations, disappearance of a few less dominant peaks and changes in FWHM are observed. The variation in peak position and peak intensity may be correlated with the extent of doping. At high doping concentration the FWHM increased, which indicates degradation of crystallinity and strain induced defects.

Morphological Studies

SEM images of the Eu doped Cu_2O thin films are shown in Fig. 2. The doped Eu element showed an effect in the morphology of the film as we can easily see in Fig. 2a, b and c. Morphology of the films has a cauliflower-like structure for Eu-doped copper oxide thin films. Figure 2a, b and c shows increased grain size of the doped Cu_2O thin films with respect to Eu doping %. As shown in Fig. 2c, a cauliflower-like shape is formed by increasing Eu doping concentration to 5%. The inset of Fig. 2c displays a cross-sectional SEM image of the film Cu_2O film coated with 5% Eu concentration. Also observed is the formation of spherically shaped particles on the substrate. These SEM images reveal that the film surface is constructed by the uniformly sized grains, which are formed due to the agglomeration of crystallites. The embedded particles in agglomerated spheres of Cu_2O of 5% Eu-doped samples may be due to the increase of Europium atoms that tend to occupy the surface.[26] ZnO film has a hexagonal and leaf shaped grains as shown in Fig. 2d. Energy dispersive analysis of x-ray (EDAX) spectrum of the heterojunction structure is shown in Fig. 3. The EDAX spectra confirms the presence of europium, copper and oxygen from Eu doped Cu_2O layer, Zn and O from ZnO layer, the trace of In and Sn may be due to ITO substrate.

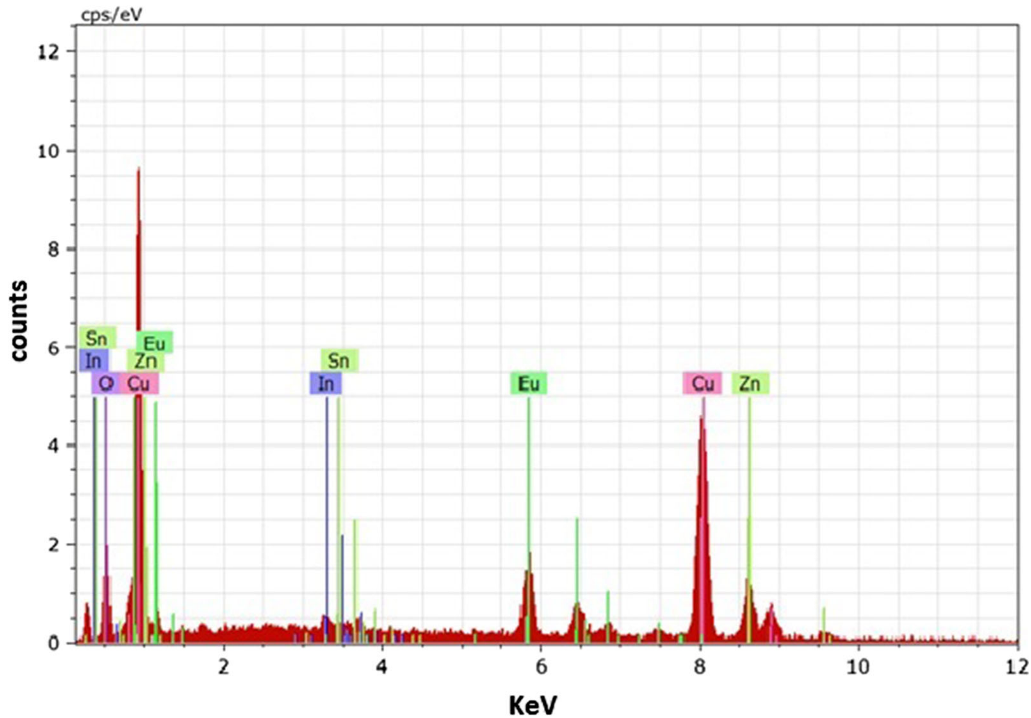

Fig. 3. EDAX spectrum of the ZnO film coated on 5% Eu-doped Cu_2O film.

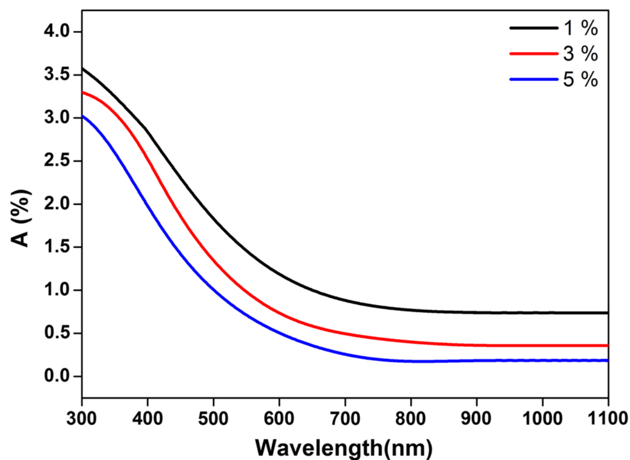

Fig. 4. Absorption spectrum of Cu_2O thin films deposited at different Eu concentrations.

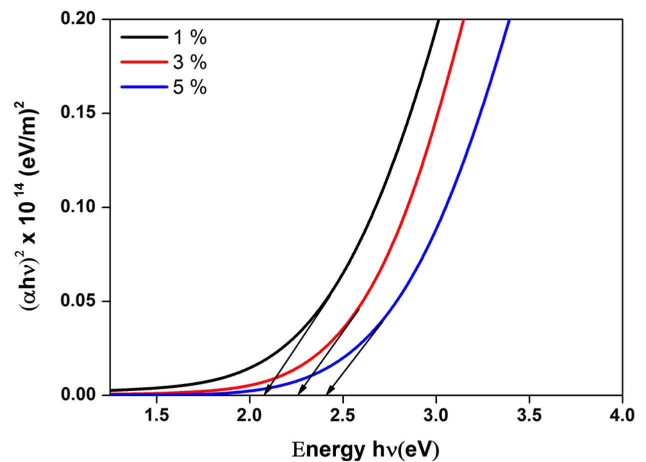

Fig. 5. Band gap of Cu_2O thin films deposited at different Eu concentrations.

Optical Studies

Absorbance spectra of Eu-doped (1%, 3% and 5%) Cu_2O thin films are shown in Fig. 4. This figure clearly shows that the absorption of Eu-doped Cu_2O films is decreased with the increase of doping concentration. It shows a maximum absorbance around 425 nm and then it decreases for the increasing wavelength of the electromagnetic spectrum. This could be attributed to the fact that the sample ceases to absorb light above this wavelength.[27] The absorption edge is shifted to a lower wavelength for the increase of doping concentration due to doping induced crystalline changes as noticed from XRD and SEM results.

The optical direct energy gap of the prepared films was determined by using Tauc model and parabolic bands.[28]

$$\alpha h\nu = B(h\nu - E_g)^n \tag{6}$$

where $h\nu$ is the incident photon energy, α is the absorption coefficient, B is the constant and E_g is the optical energy gap. The direct optical energy gap of Eu doped Cu_2O thin films are shown in Fig. 5. It is clearly seen that the optical energy gap is

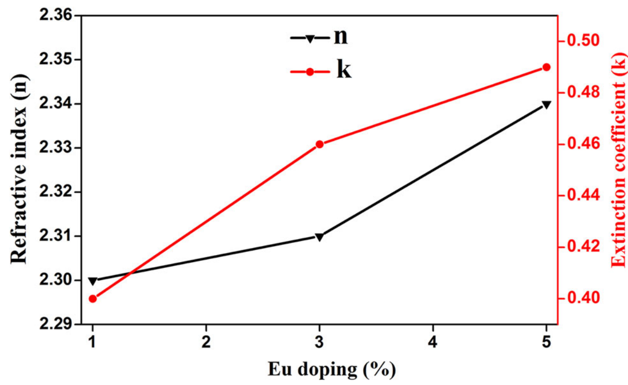

Fig. 6. Refractive index (n) and Extinction coefficient (k) of Cu_2O thin films deposited at different Eu concentration.

increased as 2.08 eV, 2.26 eV and 2.41 eV for the Eu doping concentrations of 1%, 3% and 5%, respectively. The increase of band gap with doping concentration justifies that the Eu-doped Cu_2O film is a good absorber in the UV-Vis range of solar light.[29]

The refractive index (n) values were calculated by using the below Eq. 7,[30]

$$n = \left(\frac{1+R}{1-R}\right) + \sqrt{\frac{4R}{(1-R)^2}} - K^2 \qquad (7)$$

Extinction coefficient (k) determined by using Eq. 8,[30]

$$k = \frac{\alpha\lambda}{4\pi} \qquad (8)$$

Equations 10 and 11 were used to estimate the real (ε_r) and imaginary part (ε_i) of the dielectric constants.[31]

$$\varepsilon = \varepsilon_1 + i\varepsilon_2 \qquad (9)$$

$$\varepsilon_1 = n^2 - k^2 \qquad (10)$$

$$\varepsilon_2 = 2nk \qquad (11)$$

where k is the extinction coefficient, n is the refractive index of the material, ε_1 and ε_2 are the real and imaginary part of dielectric constants, R is the reflectance (%) and λ is the wavelength in nm. Figure 6 shows the refractive index (n) and extinction coefficient (k) of Cu_2O thin films deposited at different Eu doping concentrations. The refractive index value is increased with the Eu doping due to the increase of film thickness. A lower extinction coefficient value is obtained for the film deposited at 1% Eu doping concentration. In intrinsic material property the dielectric constant is known to be fundamental. Usually, the real part is connected to slowing down the speed of light in the material.

The real part of dielectric constant is found to be higher for the 5% Eu-doped film; this is due to the favorable value of refractive index (Fig. 7). The real part is related to the dispersion, while the imaginary part estimates the dissipative rate of the wave in the medium.

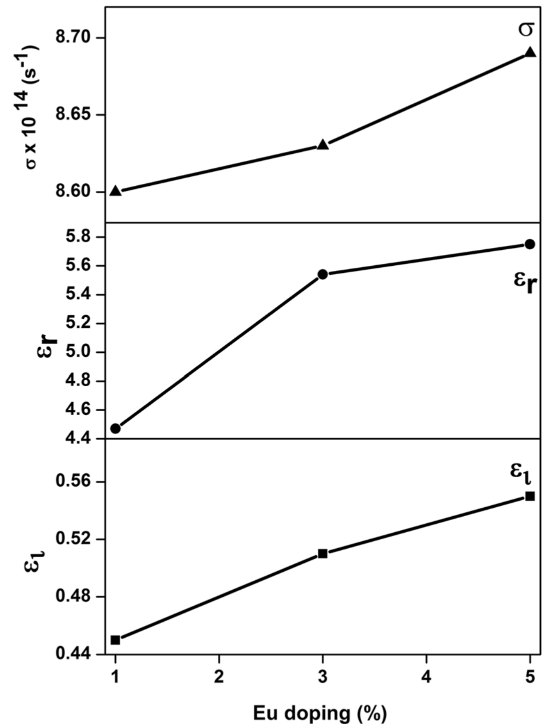

Fig. 7. Real and imaginary parts of dielectric constant and optical conductivity of Cu_2O thin films.

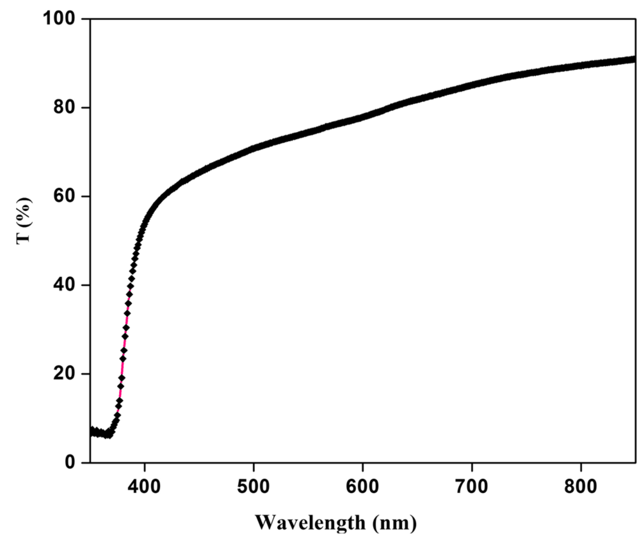

Fig. 8. Transmission spectrum of SILAR-deposited ZnO thin film.

The optical conductivity (σ) was calculated using the below Eq. 12,[32]

$$\sigma = \alpha\, n\, c \qquad (12)$$

The optical conductivity of the copper oxide thin films prepared with different Eu doping is shown in

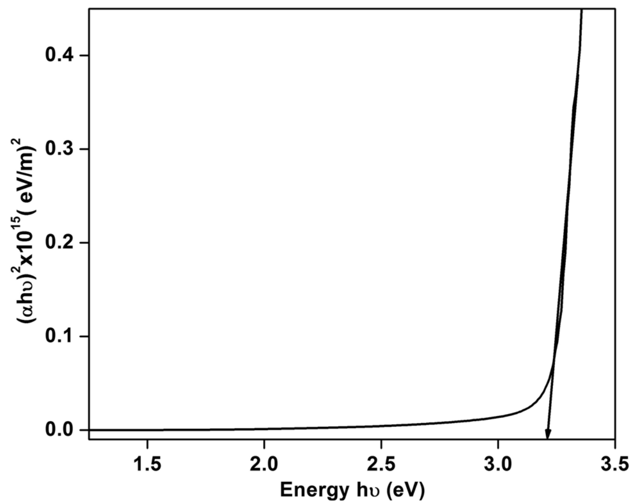

Fig. 9. Band gap of SILAR-deposited ZnO thin film.

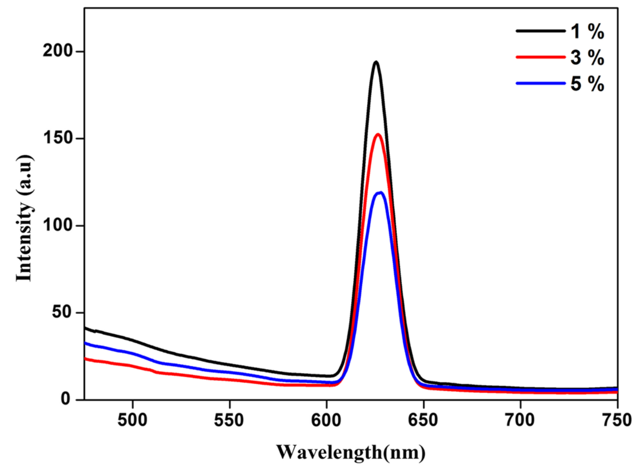

Fig. 10. Photoluminescence spectrum of Eu:Cu_2O thin films.

Fig. 7. The optical conductivity values appear to be enhanced due to the high absorbance at high photon energies.

Figure 8 shows the transmittance spectrum of ZnO film. It shows a value of transmittance around 80% in the visible range. Figure 9 shows the band gap of ZnO thin film deposited by SILAR. The obtained band gap value of ZnO is 3.20 eV, which is perfectly matched with band gap value reported for ZnO.[33]

Photoluminescence Study

Photoluminescence analysis was carried out at room temperature. The photoluminescence spectra were recorded by exciting the sample with a laser of wavelength 325 nm. It is found to be composed of a sharp emission peak around 615 nm associated with the direct exciton recombination (X_0-line), as shown in Fig. 10. Phonons are not usually participating in such transitions.[34,35] The highest peak intensity is observed for 1% Eu doping.

PL spectrum of the ZnO thin film recorded with excited wavelength 325 nm at room temperature is shown in Fig. 11. The PL spectrum of ZnO thin film exhibits one strong and one broad emission peak. Generally, the emission band is due to the recombination of bound excitons in ZnO. The first strongest peak localized at around 376 nm corresponds to exciton recombination. In addition, another intense peak is placed at 550 nm, which is due to oxygen vacancies or Zn interstitial.[36] This PL emission peak observed at 376 nm may be associated with NBE, which is in accordance with the reported value.[37] A broad shoulder peak located at 425 nm may be due to the defects in the crystalline nature of ZnO structure.[36]

Electrical Properties Analysis

The variation of electrical resistivity with Eu doping concentration in Cu_2O thin films is shown in Fig. 12a. Generally, the electrical conduction in Cu_2O is dominated by electrons generated from Cu interstitials and O^{2-} vacancies. In our case, it is observed that the resistivity of the Cu_2O thin films is decreased with increasing Eu doping concentration. It is due to the increase of carrier concentration by increased substitution of Eu^{3+} ions into Cu^{2+} lattices, as well as a donor, which supplies more free charge carriers for conduction mechanism. The films prepared at high 5% Eu showed a low resistivity value of 0.10×10^4 Ω-cm. A similar electrical resistivity change has been reported in the literature.[38] Figure 12b shows the variation of hall mobility and carrier concentration of doped Cu_2O thin films with different Eu doping concentration. As the Eu doping concentration increases from 1% to 5%, there is a huge increase in Hall mobility and carrier concentration. In general, the conductivity of

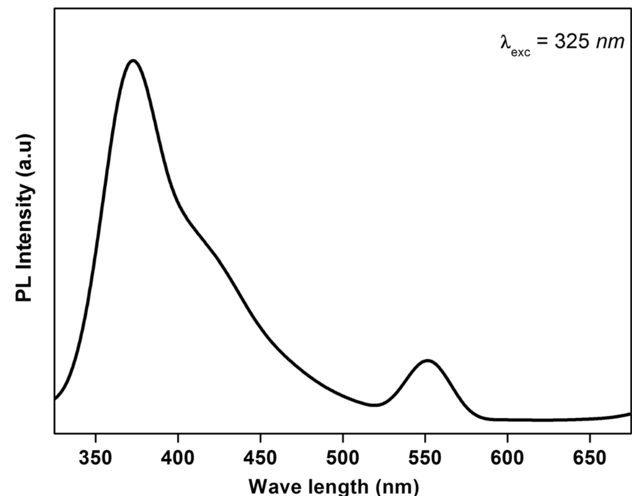

Fig. 11. Photoluminescence spectra of SILAR-deposited ZnO thin film.

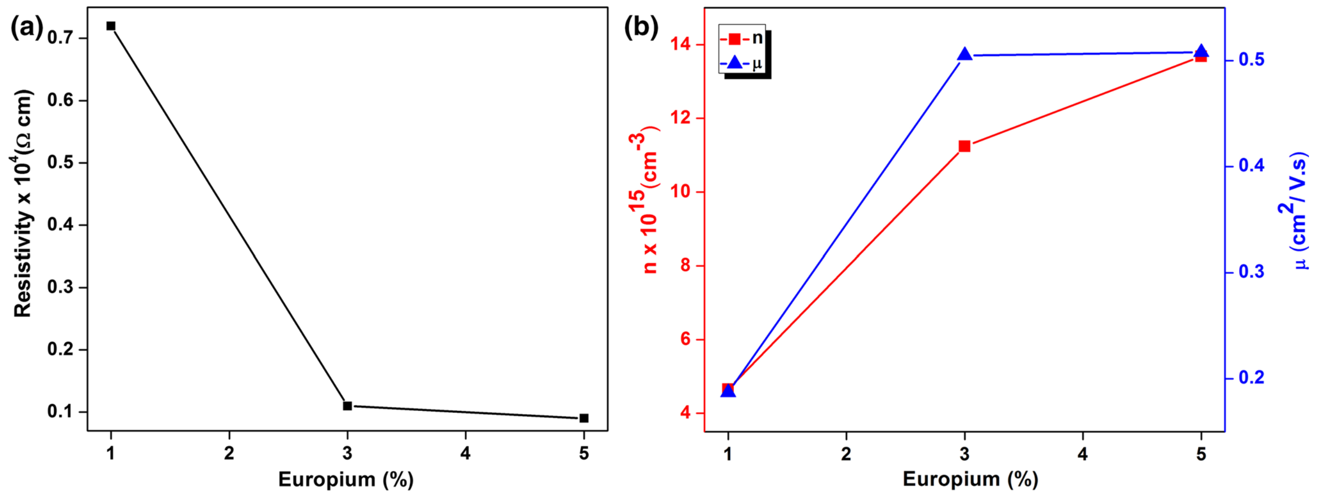

Fig. 12. (a) Resistivity and (b) Carrier concentration and Mobility for Eu doped Cu_2O films.

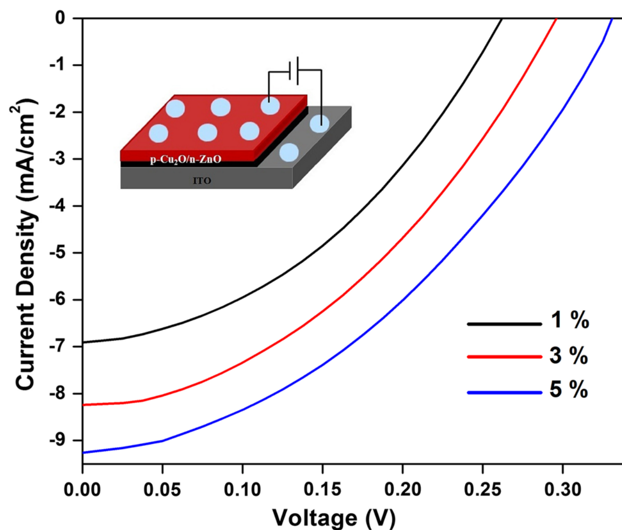

Fig. 13. Current–voltage characteristics of ITO/ZnO NRs/Eu: Cu_2O/Al cell 1%, 3% and 5% Eu doped thin films.

a semiconductor can be increased by increasing free carrier concentration. The Hall mobility and carrier concentration values of doped Cu_2O thin films at higher doping level 5% Eu are 0.52 (cm/V.s) and 13.8×10^{15} (cm^{-3}), respectively.

Solar Cell Analysis

ZnO/Cu_2O heterojunction solar cells were prepared using the same procedure as discussed in experimental part. Figure 13 shows the current density–voltage (J–V) characteristics of the heterojunction. The estimated parameters of the solar cell and their values are presented in Table II. The schematic of photovoltaic measurement in ZnO/Cu_2O heterojunction device is shown in the inset of Fig. 13. The V_{oc} is increased with increasing Eu content from 265 mV (for the pure ZnO-based device) up to 332 mV (for the device based on 5% Eu-doped Cu_2O). Moreover, the improvement of the open circuit voltage may be achieved by surface treatment of ZnO earlier to Cu_2O growth, as well as alteration in the growth conditions.[39] As shown in Fig. 13, the current density values are increased for the increase of Eu doping concentration level. The increase of current density may be due to the increase in carrier concentration, which results in the decrease of resistivity for Eu doped Cu_2O thin film; it is already discussed in electrical studies. Further, the conversion efficiency can be improved by reducing recombination centers by avoiding lattice-mismatch defects, and by reducing the resistance of Cu_2O. As the Eu^{3+} ion has the largest ionic radius (0.109 nm) compared to Cu^+ (0.077 nm), it cannot be incorporated by substitution, and instead it is incorporated as interstitial forming getter center. It suppresses the recombination losses and thus it improves current levels and increased Eu doping levels. However, this interstitial inclusion impedes the quality of crystal structure.[40] Figure 14 demonstrates the band structure and carrier transport of the fabricated *p–n* junction. As there is much difference between conduction band and valance band off-sets, a built-in potential barrier is formed, causing effective separation of charge carriers. When light is focused onto the device, photocarriers are generated and they drift to the respective electrodes depending upon the potential applied, causing current conduction. As the Eu is an

Table II. Device parameters of all solar cells tested at room temperature

Europium (%)	V_{oc} (V)	I_{sc} (mA)
1	0.265	6.89
3	0.295	8.21
5	0.332	9.24

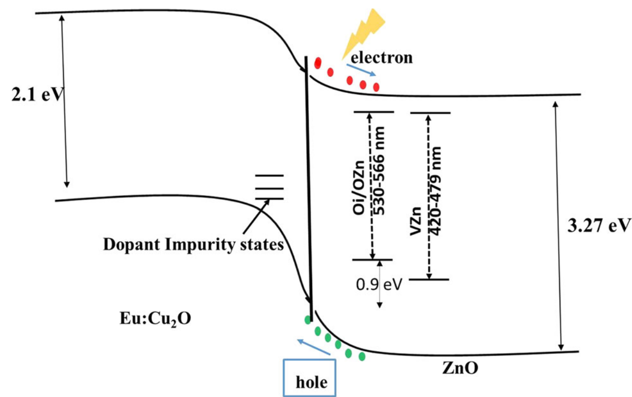

Fig. 14. Band structure and carrier transport of p–n junction.

acceptor dopant, its impurity levels are close to the valance band edge. In the case of ZnO, the green luminescence (535 nm) can be caused by the diffused Cu ion and replacing zinc. The zinc vacancy is also (VZn) in an acceptor level, which occurs at 0.8 eV. The Vo centre is at the top of the valance band. However, the ZnO coated over Eu:Cu_2O acted as a passivation layer and reduced the effect of impurity center-mediated recombination loss, improving the Voc.[41,42]

CONCLUSION

The effect of Eu doping on the Cu_2O thin films' structural, optical, morphological, and electrical and solar cell properties are discussed. Eu-doped Cu_2O and ZnO layers were deposited onto precleaned glass substrates by SILAR. Solar cell structure of ITO/ZnO/Eu:Cu_2O/Al fabricated is also characterized. The Eu-doped Cu_2O and ZnO consisted of highly oriented (111) and (002) crystallites. SEM micrographs of Eu doped Cu_2O and ZnO showed cauliflower and hexagonal morphologies, respectively. The band gap energy is increased with the increase of Eu concentration for Cu_2O films. The resistivity of the Cu_2O films is reduced to 0.10×10^4 Ω-cm for 5% Eu doping. The fabricated Eu: Cu_2O/ZnO solar cell structures showed an increased I_{sc} and V_{oc} for the increased of doping concentration, proving that doping percentage dependent the improvement in solar cell property. The best properties obtained under the experimental conditions are summarized in Table II.

ACKNOWLEDGMENTS

This work was supported by DST, India, under the scheme of Science and Engineering Research Board (SERB). DST.No. SB/FTP/PS-131/2013. The authors extend their appreciation to the Deanship of Scientific Research at King Khalid University for funding this work through research groups program under Grant Number (R.G.P.1/45/39).

REFERENCES

1. L. Colsen, F.W. Addis, and W. Miller, *Sol. Cells.* 7, 247 (1982).
2. K.P. Musselman, A. Wisnet, D.C. Iza, H.C. Hesse, C. Scheu, J.L. MacManus-Discoll, and L. Schmidt-Mende, *Adv. Mater.* 22, E254 (2010).
3. H. Tanaka, T. Shimakawa, T. Miyata, H. Sato, and T. Minami, *Appl. Surf. Sci.* 244, 568 (2005).
4. J.J. Loferski, *J. Appl. Phys.* 27, 777 (1956).
5. K. Kardarian, D. Nunes, P.M. Sberna, A. Ginsburg, D.A. Keller, J.V. Pinto, J. Deuermeier, A.Y. Anderson, A. Zaban, R. Martins, and E. Fortunato, *Sol. Energy Mater. Sol. Cells* 147, 27 (2016).
6. S.H. Wee, P.S. Huang, J.K. Lee, and A. Goyal, *Sci. Rep.* 5, 16272 (2015).
7. D.C. Perng, M.H. Hong, K.H. Chen, and K.H. Chen, *J. Alloys Compon.* 695, 549 (2017).
8. M.A. Ellah, J.P. Thomas, L. Zhang, and K.T. Leung, *Sol. Energy Mater. Sol. Cells* 152, 87 (2016).
9. K. Akimoto, S. Ishizuka, M. Yanagita, Y. Nawa, G.K. Paul, and T. Sakurai, *Sol. Energy* 80, 715 (2006).
10. N.G. Elfadill, M.R. Hashim, K.M. Chahrour, and S.A. Mohammed, *Semicond. Sci. Technol.* 31, 065001 (2016).
11. X. Yu, X. Li, G. Zheng, Y. Wei, A. Zhang, and B. Yao, *Appl. Surf. Sci.* 270, 340 (2013).
12. Y.S. Lee, J. Heo, M.T. Winkler, S.C. Siah, S.B. Kim, R.G. Gordon, and T. Buonassisi, *J. Mater. Chem.* 1, 15416 (2013).
13. L. Yu, L. Xiong, and Y. Yu, *J. Phys. Chem. C* 119, 22803 (2015).
14. N. Chander, A.F. Khan, and V.K. Komarala, *RSC Adv.* 5, 66057 (2015).
15. M.A. Hernandez-Rodríguez, M.H. Imanieh, L.L. Martín, and I.R. Martín, *Sol. Energy Mater. Sol. Cells* 116, 171 (2013).
16. K. Miura, T. Suzuki, and O. Hanaizumi, *J. Mater. Sci. Chem. Eng.* 3, 30 (2015).
17. W.J. Ho, G.C. Yang, Y.T. Shen, and Y.J. Deng, *Appl. Surf. Sci.* 365, 120 (2016).
18. J. Wu, J. Wang, J. Lin, Y. Xiao, G. Yue, M. Huang, Z. Lan, Y. Huang, L. Fan, S. Yin, and T. Sato, *Sci. Rep.* 3, 2058 (2013).
19. R. Javadi and B.D. Choi, *J. Nanosci. Nanotech.* 16, 8607 (2016).
20. M.R. Johan, M.S.M. Suan, N.L. Hawari, and H.A. Ching, *Int. J. Electrochem. Sci.* 6, 6094 (2011).
21. S.S. Nikam, M.P. Suryawanshi, S.M. Bhosale, M.A. Gaikwad, P.A. Shinde, and A.V. Moholkar, *J. Mater. Sci.: Mater. Electron.* 27, 1897 (2016).
22. M. Pal, U. Pal, J.M.G.Y. Jiménez, and F.P. Rodríguez, *Nanoscale Res. Lett.* 7, 1 (2012).
23. P.H. Klug and L.E. Alexander, *X-ray diffraction procedure* (New York: Wiley, 1954).
24. K.D.A. Kumar, S. Valanarasu, S.R. Rosario, V. Ganesh, M. Shkir, C.J. Sreelatha, and S. AlFaify, *Solid State Sci.* 78, 58 (2018).
25. M.A. Rafa and N. Rousdy, *Philos. Mag. Lett.* 90, 113 (2010).
26. M. Devika, N.K. Reddy, K. Ramesh, V. Ganesan, E.S.R. Gopal, and K.T. Ramakrishna Reddy, *Appl. Surf. Sci.* 253, 1673 (2006).
27. S.S. Oluyamo, M.S. Nyagba, and A.S. Ojo, *IOSR J. Appl. Phys.* 6, 102 (2014).
28. A.N. Banerjee, R. Maity, and K.K. Chattopadhyay, *Mater. Lett.* 58, 10 (2003).
29. N.S. Narayanan and N.K. Deepak, *Pramana. J. Phys.* 87, 87 (2016).
30. D. Sumangala, D. Amma, V.K. Vaidyan, and P.K. Manoj, *Mater. Chem. Phys.* 93, 194 (2005).
31. C. Vijayan, M. Pandiaraman, N. Soundararajan, R. Chandramohan, V. Dhanasekaran, K. Sundaram, T. Mahalingam, and J. Peter, *J. Mater. Sci.: Mater. Electron.* 22, 545 (2011).
32. K.D.A. Kumar, V. Ganesh, M. Shkir, S. AlFaify, and S. Valanarasu, *J. Mater. Sci.: Mater. Electron.* 29, 887 (2018).
33. S.V. Gastev, A.A. Kaplyanskii, and N.S. Sokolov, *Solid State Commun.* 42, 389 (1982).

34. T. Ito and T. Masumi, *J. Phys. Soc. Jpn.* 66, 2185 (1997).
35. K.D.A. Kumar, S. Valanarasu, A. Kathalingam, V. Ganesh, M. Shkir, and S. AlFaify, *Appl. Phys. A* 123, 801 (2017).
36. D.J. Edison, W. Nirmala, K.D.A. Kumar, S. Valanarasu, V. Ganesh, M. Shkir, and S. AlFaify, *Phys. B* 523, 31 (2017).
37. M. Rasadujjaman, M. Shahjahan, M.K.R. Khan, and M.M. Rahman, *SUST J. Sci. Technol.* 20, 1 (2012).
38. J. Cui, *J. Phys. Chem. C* 114, 6408 (2010).
39. S. Jung, S. Ahn, J. Yun, J. Gwak, D. Kim, and K. Yoon, *Curr. Appl. Phys.* 10, 990 (2010).
40. J. Katayama, K. Ito, M. Matsuoka, and J. Tamaki, *J. Appl. Electrochem.* 34, 687 (2004).
41. S. Shyamal, P. Hajra, H. Mandal, A. Bera, D. Sariket, A.K. Satpati, M.V. Malashchonak, A.V. Mazanik, O.V. Korolik, A.I. Kulak, E.V. Skorb, A. Maity, E.A. Streltsov, and C. Bhattacharya, *Chem. Eng. J.* 335, 676 (2018).
42. N.H. Ke, P.T.K. Loan, D.A. Tuan, H.T. Dat, C.V. Tran, and L.Y.T. Hung, *J. Photochem. Photobiol. A Chem.* 349, 100 (2017).

Publisher's Note Springer Nature remains neutral with regard to jurisdictional claims in published maps and institutional affiliations.